ACS APPLIED MATERIALS & INTERFACES

Research Article

www.acsami.org

Theoretical Study of Light Trapping in Nanostructured Thin Film Solar Cells Using Wavelength-Scale Silver Particles

Ali Dabirian*[,†,‡] and Nima Taghavinia[‡]

[†]Photovoltaics and Thin Film Electronics Laboratory, Ecole Polytechique Fédérale de Lausanne (EPFL), Rue de la Maladière 71, Neuchatel 2000, Switzerland

[‡]Department of Physics, Sharif University of Technology, Tehran 14588, Iran

Supporting Information

ABSTRACT: We propose and theoretically evaluate a plasmonic light trapping solution for thin film photovoltaic devices that comprises a monolayer or a submonolayer of wavelength-scale silver particles. We systematically study the effect of silver particle size using full-wave electromagnetic simulations. We find that light trapping is significantly enhanced when wavelength-scale silver particles rather than the ones with subwavelength dimensions are used. We demonstrate that a densely packed monolayer of spherical 700 nm silver particles enhances integrated optical absorption under standard air mass 1.5 global (AM1.5G) in a 7 μm-thick N719-sensitized solar cell by 40% whereas enhancement is smaller than 2% when 100 nm ones are used. Superior performance of wavelength-scale silver particles is attributed to high-order whispering gallery modes that they support. These modes scatter the light over a wider angular range, hence increasing the density of both waveguide and resonance modes within the dye-sensitized layer.

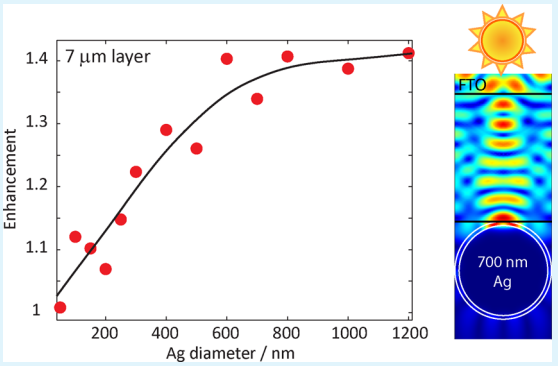

KEYWORDS: *thin film solar cell, light trapping, plasmonic, dye-sensitized solar cell, light scattering*

INTRODUCTION

Nanostructured thin film photovoltaics technologies, such as dye-sensitized solar cells (DSCs),[1,2] quantum-dot solar cells,[3] and perovskite solar cells,[4−6] present a low-cost alternative to the ubiquitous crystalline silicon solar cells with potential applications in building integrated photovoltaics (BIPV)[7] and consumer electronics products.[8] Using thin films has several advantages including the possibility of making cells mechanically flexible and partially transparent. However, these advantages bring along incomplete or insignificant light absorption in the cell. Therefore, light trapping or light management techniques have been strongly pursued for these solar cells. Traditionally thick scattering layers composed of wavelength-scale anatase,[9] rutile,[10] or core−shell particles[11] have been used to trap light inside DSCs. These scattering layers provide the most efficient light trapping; however, they suffer from two drawbacks: (i) they need to be thick enough in the range of tens of microns, which leads to difficulty in making the cell mechanically flexible, and (ii) they make the cell opaque. Therefore, alternative light trapping solutions such as photonics crystals and embedded scattering particles, although with lower efficiency in light trapping, have been used to keep the cell either transparent or thin enough for flexible applications.

Plasmonic enhanced light absorption[12,13] is a topic that has been strongly pursued in photovoltaics; however, the actual enhancements reported in high-efficiency devices have been rare.[14−16] A large part of the low performance of plasmonic light trapping schemes in action lies in the optical absorption in the metal, which is a source of energy dissipation. Entirely inhibiting the plasmonic losses is impossible; however, increasing the ratio of scattering to absorption cross-section of plasmonic particles is possible by simply enlarging the particles to wavelength-scale dimensions, i.e., several hundreds of nanometers.[17−19]

Here we show that wavelength-scale plasmonic particles with improved scattering to absorption cross-section can provide a viable light trapping solution, suitable for nanostructured solar cells. We use full-wave electromagnetic optical simulation to evaluate optical absorption in a DSC with a monolayer of SiO_2-coated silver particles placed at the dye-sensitized layer and the electrolyte (DSL/EL) interface. We investigate the effect of silver particle size, size distribution, surface coverage, and the possibility of multilayer formation on the optical absorption in the sensitized layer of DSC. Absorption enhancement dramatically increases when wavelength-scale silver particles are used. We investigate the mechanism of enhanced light absorption in the device in relation to resonance and waveguide modes of the dye-sensitized layer. We also compare the optical absorption of the layer to Yablonovitch or $4n^2$ limit of optical

Received: April 29, 2015
Accepted: June 22, 2015
Published: July 2, 2015

DOI: 10.1021/acsami.5b03719
ACS Appl. Mater. Interfaces 2015, 7, 14926−14932

absorption in thin films.[20] Then, on the basis of the electromagnetic field profiles we confirm the light coupling to guided modes of dye-sensitized layers. In addition, on the basis of our data, we draw general conclusions on the superior performance of sub-micron-scale plasmonic particles in light trapping in thin film solar cells relative to subwavelength plasmonic particles.

CELL CONFIGURATION AND SIMULATION METHOD

The reference structure is a standard DSC, which usually comprises a mesoporous TiO_2 layer composed of 15−20 nm basic particles coated on a SnO_2:F (FTO)-coated glass.[2] We consider a mesoporous layer that is sensitized with N719 dye molecules, and it is completely infiltrated with either a liquid or a solid electrolyte. The scattering layer comprises an ordered array of silver particles of circular cross-section that are coated with 30 nm SiO_2 layer placed at the DSL/EL interface (Figure 1a). We consider the SiO_2 coating in our calculations because it

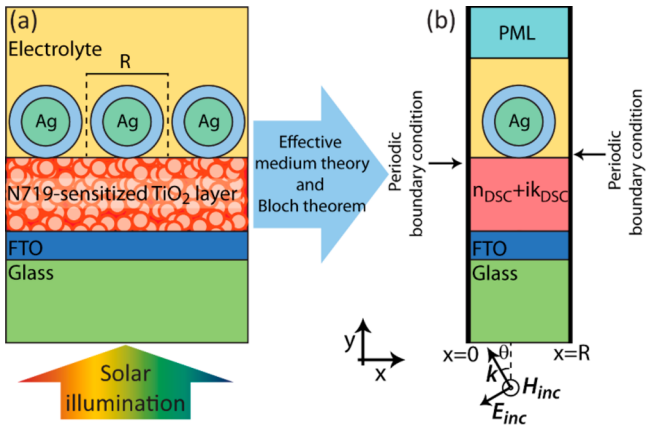

Figure 1. (a) Schematic of a standard DSC having an array of Ag@SiO_2 particles on top. The light impinges on the cell from the FTO side, which is the normal configuration in DSCs. (b) Schematic of a computational domain used in our FEM electromagnetic optical simulations. It consists of a unit cell of the DSC in which the dye-sensitized layer is modeled as a layer with an effective complex refractive index. The computational domain is restricted by periodic boundary conditions from the sides and by the perfectly matched layer (PML) from the top.

is often used to isolate silver from the semiconductor to avoid charge recombination and also to prevent corrosion of silver in the electrolyte. We assume sunlight illumination from the glass side in our calculations, which is the standard configuration of DSC operation.

The complex refractive index data of the N719-sensitized mesoporous TiO_2 layer are obtained from ref 2, where the effective refractive index of 1.9 and absorption coefficient of 2.83×10^{-3} cm^{-1} at 532 nm were reported. Therefore, in our modeling we approximate the N719-sensitized layer with a dense layer of refractive index 1.9 and extinction coefficient k that is obtained by weighting the normalized dye molar absorptance spectrum with the coefficient determined by the absorption coefficient of the sensitized layer at 532 nm. Subwavelength (<20 nm) dimensions of TiO_2 nanoparticles justify this effective medium approximation. The mesoporous TiO_2 and the electrolyte partially absorb the light; however, for simplicity we ignore these effects in all of our simulations. The complex refractive index data of Ag are obtained from the data reported in ref 21.

We calculate the electromagnetic fields inside the cell by solving full-field Maxwell equations over the entire cell. All effects related to electromagnetic fields including near-field, radiating near-field, and scattered (or far-field) effects are taken into account in such simulations. Sunlight illumination is treated as a plane-wave with an angle of incidence θ, and wave-vector $\vec{k} = k_0(-\sin\theta\hat{x} + \cos\theta\hat{y})$,[24] where $k_0 = \omega_0/c$. Polarization of the incident light is such that the magnetic field is directed out of the page. Thomann et al.[22] have confirmed that the predictions obtained under this polarization of light incidence show close agreement with experimental results obtained when silica-coated plasmonic nanoparticles are used. Nevertheless, we conducted calculations for the other polarization in which the electric field is out of plane to have an estimation of the enhancement in this case too (Supporting Information, Figure S1).

The scattering layer is periodic along the x-axis; therefore, in our finite element method (FEM) simulations the computational domain contains only a unit cell of the structure as depicted in Figure 1b. On the left and the right sides of the computational domain, periodic boundary conditions, also called Floquet or Bloch boundary conditions, are applied. These boundary conditions basically imply that across the computation domain the electromagnetic fields are related by $\vec{E}(\vec{H})(x = R) = \vec{E}(\vec{H})(x = 0) \times \exp(-ik_0 x \sin\theta)$. From the electrolyte the computational domain is truncated by a perfectly matched layer (PML). PML is a fictitious material that is used in computational electromagnetics to simulate the boundary conditions for a half-space.[23] Basically it absorbs the entire incident light over every incidence angle hence establishing a reflection-free condition. From the FEM simulations we calculate the electromagnetic fields $\vec{E}$ and $\vec{H}$ at every point within the DSC structure. Optical absorption within the sensitized layer of DSC is then calculated as the dissipation of electromagnetic energy inside this layer described by $A(\lambda) = (1/P_{inc}) \times \int (1/2)\omega''_{DSC}|E(\bar{r}, \lambda)|^2 \, d^3r$ where $|E(\bar{r}, \lambda)|$ is the amplitude of electric field, ω''_{DSC} is the imaginary part of the effective dielectric constant of N719-sensitized mesoporous TiO_2 layer, and P_{inc} is the power carried by the incident wave. The integration is carried out over the entire volume of the N719-sensitized layer of DSC. This dissipation, caused by ω''_{DSC}, describes the rate of vibronic transition from the HOMO to LUMO taking place in the dye molecule. Therefore, it is directly related to the rate of generation of electrons due to light absorption.

The absorption spectrum is then weighted by the AM1.5 solar spectrum to calculate the rate at which electrons are generated under standard solar illumination. With the help of the Planck formula for energy of a photon, $E = hc/\lambda$, the rate of electron generation under AM1.5 sunlight illumination is calculated as $J_a = (e/hc)\int A(\lambda)\Phi_{AM1.5}\lambda \, d\lambda$ where $\Phi_{AM1.5}$ describes the AM1.5 irradiance and λ is the wavelength.[24,25] The unit of J_a is mA cm^{-2}, and it describes the maximum achievable current density in the cell.[10] The J_a is related to the short-circuit current density of the cell (J_{SC}) through $J_{SC} = J_a \times \eta_{inj} \times \eta_{reg} \times \eta_{coll}$, where η_{inj} describes the electron injection efficiency, η_{reg} describes the dye regeneration efficiency, and η_{coll} describes the charge collection efficiency.[26]

We evaluate the performance of the scattering layer by comparing the performance of a cell with the Ag scattering layer on top against the standard cell, and also against the

DOI: 10.1021/acsami.5b03719
ACS Appl. Mater. Interfaces 2015, 7, 14926−14932

reference cell having a perfect electric conductor reflector with 100% specular reflectance on top. In this way, we basically compare these plasmonic scatterers with the upper limit of widely used TiO_2 scatterers or Ag backreflectors made from a dense and shiny Ag thin film.

RESULTS AND DISCUSSION

Figure 1a shows the enhancements in J_a of a DSC with a monolayer of densely packed Ag@SiO_2 particles on top as the size of the Ag scatterers varies from 100 to 1200 nm. The calculations are performed for DSCs having either 1 or 7 μm-thick N719-sensitized layers whereas all other parameters of the cell were kept fixed. Figure 2a,b shows the J_a enhancements due to Ag@SiO_2 particles and also due to an ideal 100% reflector used instead of the Ag@SiO_2 particles. As the size of Ag@SiO_2 particles increases from 100 nm the enhancement increases rapidly; however, it reaches a slowly increasing plateau as the dimension of Ag@SiO_2 particles approaches 600 nm. These wavelength-scale Ag@SiO_2 particles outperform the ideal reflector delivering larger enhancements in both 1 and 7 μm-thick DSCs.

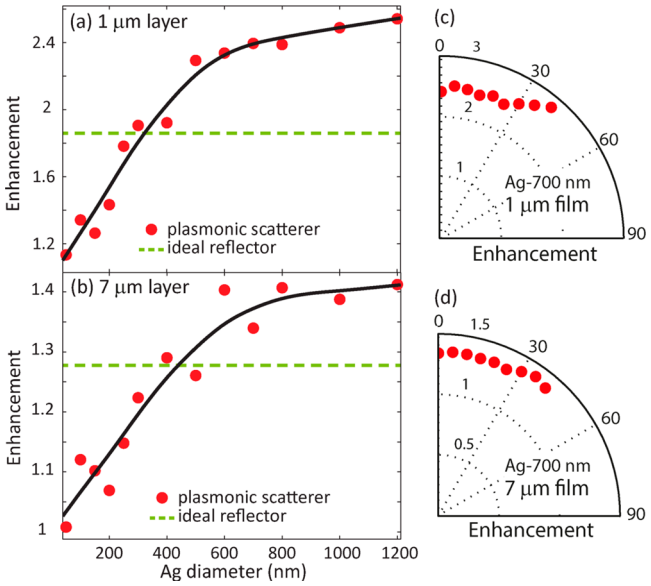

Figure 2. J_a enhancement of the DSCs having (a) 1 and (b) 7 μm-thick N719-sensitized layers versus the size of Ag particles after using either a monolayer of densely packed Ag@SiO_2 particles on top of an ideal reflector. The black line is a numerical fit to the red dots, and it is to guide the eyes. The J_a enhancements obtained at different angles of incidence in DSCs with (c) 1 and (d) 7 μm-thick N719-sensitized layers when a densely packed monolayer of 700 nm Ag particles is used.

The enhancements in J_a of DSC with 1 μm-thick N719-sensitized layer are significantly large, reaching nearly 2.4-fold enhancements when Ag@SiO_2 particles larger than 500 nm are used. However, the enhancements reach 40% in DSC with 7 μm-thick N719-sensitized layers. In general, the enhancements decrease as the thickness of the dye-sensitized layer increases (Supporting Information, Figure S2) because in thick layers a larger portion of light is absorbed within the layer before it interacts with the particles monolayer.

For solar panels to be able to keep their high efficiency also for diffuse illumination in cloudy days and during all daytime hours they need to maintain their performance at large angles of light incidence. Figure 2c,d shows the J_a enhancements calculated for 1 and 7 μm-thick DSCs each having a densely packed monolayer of 700 nm Ag particles on top as the incidence angle is varied from 0° to 45° from the normal incidence. One can see that in both cases the enhancements are even slightly improved at larger angles of light incidence. The circular shape of the Ag@SiO_2 particles comprises the main reason for their wide angular acceptance.

The depth at which the Ag@SiO_2 particles are partially embedded in the absorbing layer does not show significant influence on the J_a enhancements (Figure 3). Therefore, we can conclude that the enhancement is largely due to light scattering from Ag@SiO_2 particles and not to the near-field enhancement effects. If the near-field enhancement is the dominant mechanism, the depth at which the Ag@SiO_2 particles are embedded in the absorbing layer is highly influential because it affects overlap of the near-fields with the light absorbing materials.[12] To further evaluate the performance of these particles and study the enhancement mechanism we limit our investigation to 100 and 700 nm Ag particles with a 30 nm silica insulating shell.

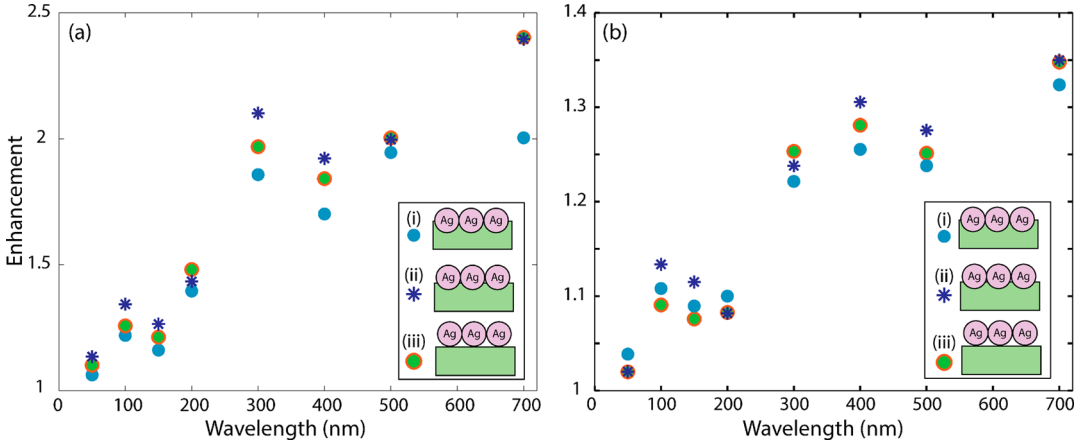

Figure 3. Enhancements in J_a of DSC with (a) 1 and (b) 7 μm-thick N719-sensitized layer versus the size of Ag@SiO_2 particles at three different configurations: (i) half-embedded, (ii) quarter-embedded, and (iii) not embedded Ag@SiO_2 particles on the surface. The data suggest that the depth of the scatters does not have a dramatic influence on the enhancements, and in all three configurations the trend of enhancement with particle size is the same.

DOI: 10.1021/acsami.5b03719
ACS Appl. Mater. Interfaces 2015, 7, 14926−14932

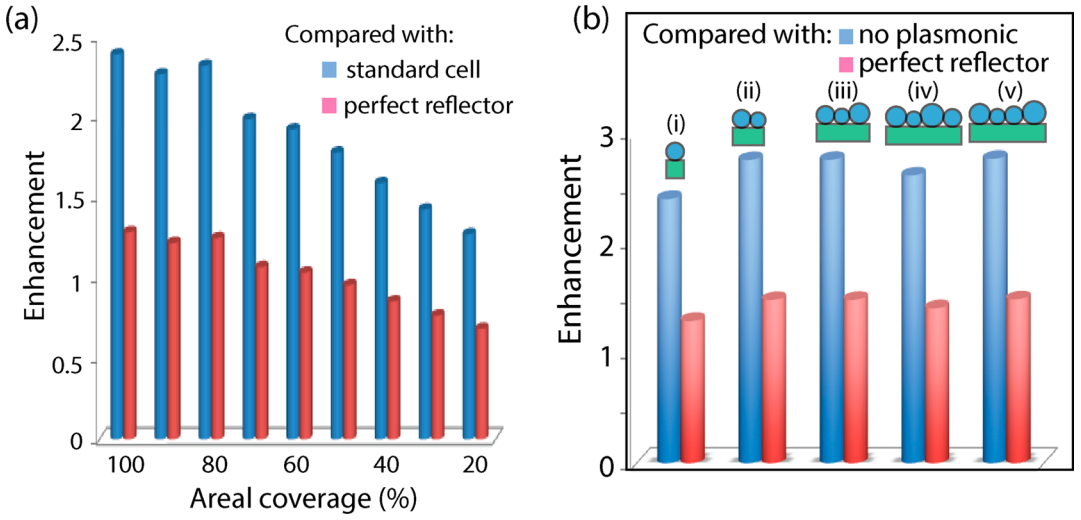

Figure 4. J_a enhancements obtained in DSCs with 1 μm-thick N719-sensitized layers (a) when different areal coverages of 700 nm Ag particles are used and (b) when a unit cell of the densely packed scattering layer comprises (from left to right) (i) 700 nm; (ii) 700, 600 nm; (iii) 700, 600, 800 nm; (iv) 800, 600, 900, 700 nm; and (v) 800, 600, 700, 900 nm Ag particles. Enhancements are obtained relative to a standard DSC and a DSC having an ideal reflector.

In experimental realization of this light trapping solution two effects occur: (i) the established processes for synthesis of Ag nanoparticles result in particles of a certain size distribution and (ii) assembly of these particles into a monolayer often results in monolayers with a certain distance among the particles. Therefore, in the following we take these effects into account in our simulations and evaluate the extent to which J_a enhancements are affected by size distribution and areal coverage of the particles. We quantify the areal coverage of Ag@SiO_2 particles as a parameter varying from 100% for a densely packed monolayer to smaller values for partially covered surfaces. Basically, areal coverage study is the same as varying the unit cell dimension of the scattering layer of Ag@SiO_2 particles.

Figure 4a shows the enhancements in J_a obtained for 700 nm Ag particles atop a DSC having 1 μm-thick N719-sensitized layer relative to the standard DSC and the DSC with ideal reflector as partial coverage of the particles varies from 20% to 100%. The J_a enhancements are not significantly influenced for partial coverage down to 80%; however, they deteriorate as the areal coverage of Ag@SiO_2 particles on the surface decreases further. In principle, when the spacing between the particles is small the light cannot pass through due to the diffraction limit,[27] unless it couples to the plasmonic modes. Therefore, in a comparison to a densely packed monolayer of Ag@SiO_2 particles, small spacing between Ag@SiO_2 particles does not add an extra channel for light to pass through. However, when the spacing between the particles is larger than the diffraction limit, then the light can pass through, and the larger the spacing becomes the larger amount of light passes through. Thus, we observe that J_a enhancements deteriorate as the areal coverage of Ag@SiO_2 particles on the surface drops below 80%. Down to 50% areal coverage, the submonolayer of Ag@SiO_2 particles still outperforms the perfect reflector.

To determine the influence of the size distribution of Ag@SiO_2 particles, we evaluate scattering layers composed of Ag particles of different sizes on top. Precisely, we compare five cases involving densely packed monolayers with unit cells comprising (i) 700 nm; (ii) 700, 600 nm; (iii) 700, 600, 800 nm; (iv) 800, 600, 900, 700 nm; and (v) 800, 600, 700, 900 nm Ag particles. The enhancements in J_a obtained for these five structures relative to a standard DSC and a DSC with ideal reflector are shown in Figure 4b. It shows that, as the size distribution is widened, on average, J_a enhancements increase. Therefore, in agreement with previous studies on particles,[28] our results reconfirm that broadening the size distribution of the particles does not have a negative impact on J_a enhancements.

To understand the enhancement mechanism of wavelength-scale Ag@SiO_2 particles we calculate the absorptance spectra for a standard DSC, a DSC with densely packed 100 nm Ag particles, and a DSC with densely packed 700 nm Ag particles. Thickness of the N719-sensitized layer is assumed to be either 1 or 7 μm. These spectra are also compared with the Yablonovitch limit of absorption in thin absorbers of thickness d, given by[29]

$$A_{\text{Yablonovitch}} = 1 - \frac{1}{1 + 4n^2\alpha d}$$

where n is the real part of refractive index, and α is the absorption coefficient of the N719-sensitized layer.

The absorptance spectra of a standard DSC with 1 and 7 μm-thick N719-sensitized layers are shown in Figure 5a,b, respectively. Several peaks appear in the absorptance spectra due to light interference within the layer. Basically, the absorbing layer without Ag@SiO_2 particles functions as a Fabry–Pérot resonator with partial mirrors formed by Fresnel reflection at DSL/EL and DSL/FTO interfaces. The resonator supports a set of resonance modes, also called guided resonances,[30] leading to improved optical absorption appearing as peaks in the absorptance spectrum.

The absorptance spectrum of the DSC with densely packed 100 nm Ag particles shows a larger optical absorptance over the entire wavelength range than the standard DSC does. Moreover, its spectrum shows the same number of peaks as the absorption spectrum of the standard DSC does, although with slightly blue-shifted peak positions. These peaks are attributed to the guided resonances of the absorbing layer in which light bounces back and forth within the layer as it is reflected from the top and bottom interfaces while constantly

DOI: 10.1021/acsami.5b03719
ACS Appl. Mater. Interfaces 2015, 7, 14926–14932

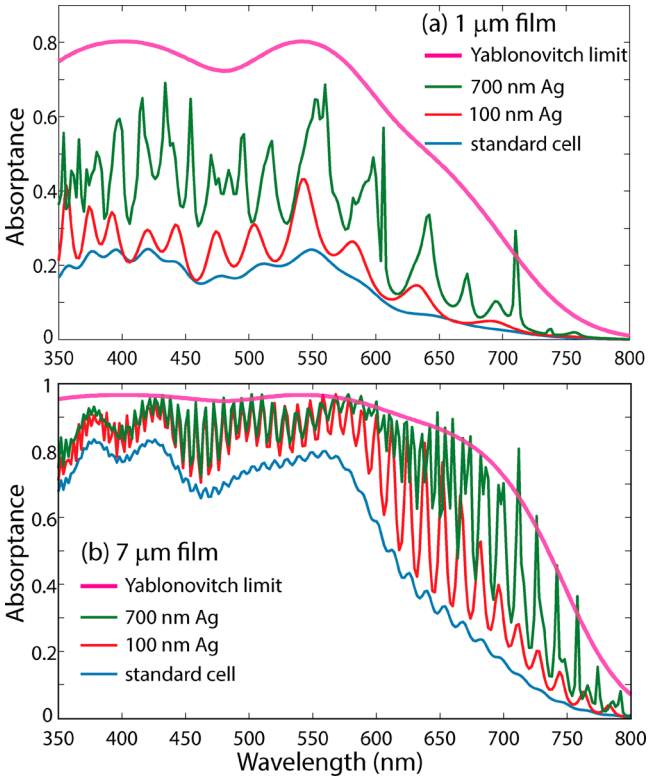

Figure 5. Calculated spectra of optical absorptance in the N719-sensitized layer of a standard DSC and a DSC having a scattering layer formed by a densely packed array of either 100 or 700 nm Ag@SiO_2 particles along with the Yablonovitch limit for absorption in (a) 1 and (b) 7 μm-thick N719-sensitized layers.

coupling parts of its energy to free-space modes outside the N719-sensitized layer. Therefore, the scattering layer of 100 nm Ag particles functions only as a top reflector with a superior reflectance as compared to that of the DSL/EL interface; however, it is far from an ideal reflector as shown in Figure 2a. The main reason for its lower performance relative to an ideal reflector is attributed to the energy losses in 100 nm Ag particles due to coupling to its localized surface plasmon resonances. Figure S3 of the Supporting Information shows the optical dissipation losses in Ag@SiO_2 particles confirming this notion.

The optical absorptance of the DSC with 700 nm Ag particles is larger than those of the DSC with 100 nm particles over the entire wavelength range. Spectra of optical absorptance of these cells show many extra peaks that appear neither in the standard DSC absorptance spectrum nor in the absorptance spectrum of the cell with 100 nm particles. This is because these larger Ag particles divert the incident light over a larger angular range. As the result, the resonance condition for the guided resonances is satisfied at many more wavelengths within the absorbing layer of the DSC. Therefore, additional guided resonance peaks appear in the absorptance spectra.

In addition to the resonance peaks, the absorptance spectra of DSCs with the 700 nm Ag particles show several sharp peaks that in some cases exceed the Yablonovitch limit. These sharp peaks designate coupling of light to the guided modes of the absorbing layer, which, in contrast to guided resonances, do not leak their energy out of the absorbing layer.[31] These modes propagate laterally within the layer until their energy is completely absorbed. A few previous articles have reported overcoming the Yablonovitch limit by coupling to the guided modes.[32,33]

To further explore the physical mechanism of larger enhancements obtained when larger Ag particles are used we calculate and compare the electric field profiles for the scattering layer formed either by 100 or 700 nm Ag particles placed atop a DSC with 1 μm-thick N719-sensitized layer. The absorbed power density is directly related to the electric field amplitude within the sensitized layer through $1/2\omega''_{DSC}|\vec{E}|^2$.

Figure 6a–c shows the profiles of the electric field amplitude at 444, 546, and 700 nm wavelengths when a densely packed

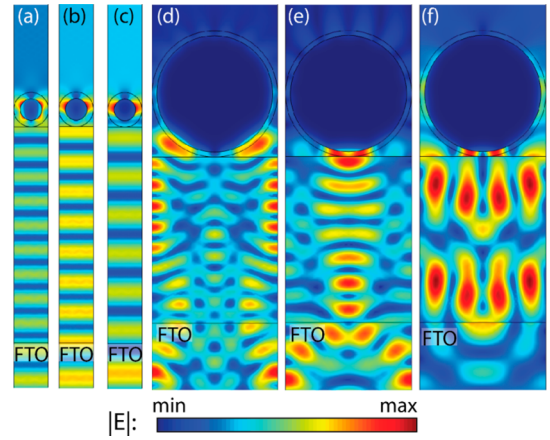

Figure 6. Calculated profiles of electric field amplitude for a DSC with 1 μm-thick N719-sensitized layer having a scattering layer formed by a densely packed monolayer of either (a–c) 100 nm or (d–f) 700 nm Ag particles coated with a 30 nm-thick silica layer placed on top. The wavelengths corresponding to the color plots are (a) 444, (b) 546, (c) 700, (d) 454, (e) 558, and (f) 710 nm. The profile shown in part f is a typical profile observed when a guided mode of the absorbing layer is excited. The other cases show the profile of guided resonances.

monolayer of 100 nm Ag particles is used on top of a DSC with 1 μm-thick N719-sensitized layer. They reveal that within the sensitized layer the electric field and essentially the wavefront remain planar in all these cases. This implies that the scattering layer formed by 100 nm Ag particles only functions as a reflector and does not influence the wavefront of the incident light. In this case, light couples to the quadrupolar (Figure 6a) and dipolar (Figure 6b,c) plasmonic resonance modes of the particles; however, the angular spread of the scattered light, in the densely packed configuration of these particles, is too small to perturb the wavefront.

Figure 6d–f shows the profiles of electric field amplitude in a DSC with a scattering layer formed by a densely packed monolayer of 700 nm particles at 454, 558, and 710 nm wavelengths. In these cases, the wavefronts are not planar anymore, but they are strongly distorted due to scattering from Ag@SiO_2 particles. The wavefront distortion takes place because the light that scatters off the monolayer of 700 nm Ag particles acquires a wide angular spread within the absorbing layer of the DSC. The scattered light can be decomposed into a set of plane waves, often called space harmonics. These space harmonics acquire a longer path length within the layer and therefore provide guided resonances with larger optical absorptions. As a result, they show a larger absorptance as compared to the guided resonances of the cell with 100 nm Ag particles (Figure 5). Moreover, space harmonics that are scattered off at angles beyond the critical angle of reflection of

DOI: 10.1021/acsami.5b03719
ACS Appl. Mater. Interfaces 2015, 7, 14926–14932

DSL/FTO interface remain trapped within the layer in the form of guided modes appearing as sharp peaks in the absorptance spectra.

The surface plasmon resonance modes of these Ag@SiO_2 particles can be described by SP^m ($\vec{E}(r, \varphi) = \vec{E}^m(r) \times \exp(\pm im\varphi)$) where m is the number of antinodes in $|\vec{E}^m(r)|$ along the silica−metal interface.[34] For instance, m, also called the angular quantum number, is 1 for a dipole mode, and it is 2 for a quadrupole mode. When the m value is large, these modes are called whispering gallery modes (WGMs), hence showing several antinodes along the silica−metal interface. In small Ag particles, the plasmonics absorption is dominant; however, at dimensions of about 100 nm the scattering efficiency becomes comparable with absorption efficiency. As the particle size becomes larger the scattering efficiency becomes significantly larger than the absorption efficiency.[19]

In principle during the scattering process light couples to these surface plasmon resonance modes of the particles, and then, the light reradiates from the particles back into the absorbing layer of the DSC. In this radiation process, the electric field profile of these resonance modes is considered as a source of secondary waves which add to produce distant wavefronts according to the surface equivalence principle or Huygens principle.[35] Given this picture of scattering from plasmonic particles, the radiated field from a high m number mode or a WGM generates distant wavefronts within the cell over a wider angular range as compared to the radiated fields of the lower m number modes such as dipole or quadrupole modes.

CONCLUSIONS

In conclusion, we have shown that the dimensions of the plasmonic particles have a significant impact on their performance to enhance sunlight absorption in DSCs with several micrometer-thick dye-sensitized layers. A monolayer of silver particles larger than 600 nm improves the AM1.5 integrated optical absorption in the DSCs with 1 and 7 μm-thick N719-sensitized layers by 150% and 40% whereas the enhancements are 18% and 2% when 100 nm silver particles are used. In addition, these large particles outperform an ideal specular reflector indicating that the particles do more than only reflect the light back into the cell. Basically, the wavelength-scale silver particles divert a portion of the light energy into larger angles prolonging their path length within the cell as well as increasing the chance of coupling to the guided modes of the dye-sensitized layer of DSC. The physical origin of all these effect lies in coupling of the light into plasmonic WGMs in wavelength-scale silver particles whereas only dipolar and quadrupolar modes are excited in 100 nm silver particles. The monolayer of wavelength-scale plasmonic particles, studied here, is a light trapping solution that is applicable to other type of nanostructured thin film solar cells.

ASSOCIATED CONTENT

Supporting Information

Simulation results under TE polarized light, enhancement as the function of layer thickness, and angular behavior of enhancement. The Supporting Information is available free of charge on the ACS Publications website at DOI: 10.1021/acsami.5b03719.

AUTHOR INFORMATION

Corresponding Author

*E-mail: ali.dabirian@epfl.ch.

Notes

The authors declare no competing financial interest.

REFERENCES

(1) O'Regan, B.; Grätzel, M. A Low-Cost High-Efficiency Solar-Cell Based on Dye-Sensitized Colloidal TiO_2 Films. *Nature* **1991**, *353*, 737−740.
(2) Grätzel, M. Solar Energy Conversion by Dye-Sensitized Photovoltaic Cells. *Inorg. Chem.* **2005**, *44*, 6841−6851.
(3) Lee, Y.-L.; Lo, Y.-S. Highly Efficient Quantum-Dot-Sensitized Solar Cell Based on Co-Sensitization of CdS/CdSe. *Adv. Funct. Mater.* **2009**, *19*, 604−609.
(4) Lee, M. M.; Teuscher, J.; Miyasaka, T.; Murakami, T. N.; Snaith, H. J. Efficient Hybrid Solar Cells Based on Meso-Superstructured Organometal Halide Perovskites. *Science* **2012**, *338*, 643−647.
(5) Liu, M.; Johnston, M. B.; Snaith, H. J. Efficient Planar Heterojunction Perovskite Solar Cells by Vapour Deposition. *Nature* **2013**, *501*, 395−398.
(6) Burschka, J.; Pellet, N.; Moon, S.-J.; Humphry-Baker, R.; Gao, P.; Nazeeruddin, K.; Grätzel, M. Sequential Deposition as a Route to High-Performance Perovskite-Sensitized Solar Cells. *Nature* **2013**, *499*, 316−319.
(7) Pagliaro, M.; Ciriminna, R.; Palmisano, G. BIPV: Merging the Photovoltaic with the Construction Industry. *Prog. Photovoltaics* **2010**, *18*, 61−72.
(8) Hinsch, A.; Veurman, W.; Brandt, H.; Jensen, K. F.; Mastroianni, S. Status of Dye Solar Cell Technology as a Guideline for Further Research. *ChemPhysChem* **2014**, *15*, 1076−1087.
(9) Dadgostar, S.; Tajabadi, F.; Taghavinia, N. Mesoporous Submicrometer TiO_2 Hollow Spheres as Scatterers in Dye-Sensitized Solar Cells. *ACS Appl. Mater. Interfaces* **2012**, *4*, 2964−2968.
(10) Lin, J.; Heo, Y.-U.; Nattestad, A.; Shahabuddin, M.; Yamauchi, Y.; Kim, J. H. N719- and D149-Sensitized 3D Hierarchical Rutile TiO_2 Solar Cells—A Comparative Study. *Phys. Chem. Chem. Phys.* **2015**, *17*, 7208−7213.
(11) Gazyani, N.; Majles Ara, M.; Tajabadi, F.; Dabirian, A.; Mohammadpour, R.; Tagavinia, N. Dielectric Core−Shells with Enhanced Scattering Efficiency as Back-Reflectors in Dye Sensitized Solar Cells. *RSC Adv.* **2014**, *4*, 3621−3626.
(12) Atwater, H. A.; Polman, A. Plasmonics for Improved Photovoltaic Devices. *Nat. Mater.* **2010**, *9*, 205−213.
(13) Polman, A.; Atwater, H. A. Photonic Design Principles for Ultrahigh-Efficiency Photovoltaics. *Nat. Mater.* **2012**, *11*, 174−177.
(14) Ding, I.-K.; Zhu, J.; Cai, W.; Moon, S.-J.; Cai, N.; Wang, P.; Zakeeruddin, S. M.; Grätzel, M.; Brongersma, M. L.; Cui, Y.; McGehee, M. D. Plasmonic Dye-Sensitized Solar Cells. *Adv. Eenergy Mater.* **2011**, *1*, 52−57.
(15) Choi, H.; Chen, W. T.; Kamat, P. V. Know Thy Nano Neighbor. Plasmonic versus Electron Charging Effects of Metal Nanoparticles in Dye-Sensitized Solar Cells. *ACS Nano* **2012**, *6*, 4418−4427.
(16) Ferry, V. E.; Munday, J. N.; Atwater, H. A. Design Considerations for Plasmonic Photovoltaics. *Adv. Mater.* **2010**, *22*, 4794−4808.
(17) Ruan, Z.; Fan, S. Scattering of Light from Subwavelength Nanostructures. *Phys. Rev. Lett.* **2010**, *105*, 013901 (1−4).
(18) Cushing, S. K.; Wu, N. Plasmon-Enhanced Solar Energy Harvesting. *Electrochem. Soc. Interface* **2013**, *22*, 63−67.
(19) Tribelsky, M. I.; Luk'yanchuk, B. S. Anomalous Light Scattering by Small Particles. *Phys. Rev. Lett.* **2006**, *97*, 263902 (1−4).
(20) Yablonovitch, E. Statistical Ray Optics. *J. Opt. Soc. Am.* **1982**, *72*, 899−907.
(21) Weber, M. J. *Handbook of Optical Materials*; CRC Press: Boca Raton, FL, 2003.

DOI: 10.1021/acsami.5b03719
ACS Appl. Mater. Interfaces 2015, 7, 14926−14932

(22) Thomann, I.; Pinaud, B. A.; Chen, Z.; Clemens, B. M.; Jaramillo, T. F.; Brongersma, M. L. Plasmon Enhanced Solar-to-Fuel Energy Conversion. *Nano Lett.* **2011**, *11*, 3440−3446.
(23) Berenger, J.-P. Three-Dimensional Perfectly Matched Layer for the Absorption of Electromagnetic Waves. *J. Comput. Phys.* **1996**, *127*, 363−379.
(24) Dabirian, A.; Taghavinia, N. Resonant-Size Spherical Bottom Scatterers for Dye-Sensitized Solar Cells. *RSC Adv.* **2013**, *3*, 25417−25422.
(25) Dabirian, A. Extreme Light Absorption in a Necking-Free Monolayer of Resonant-Size Nanoparticles for Photoelectrochemical Cells. *J. Opt.* **2014**, *16*, 075001 (1−7).
(26) Chandrian, A. V.; Tetreault, N.; Humphry-Baker, R.; Kessler, F.; Baranoff, E.; Yi, C.; Nazeeruddin, M. K.; Grätzel, M. Subnanometer Ga_2O_3 Tunneling Layer by Atomic Layer deposition to Achieve 1.1 V Open-Circuit Potential in Dye-Sensitized Solar Cells. *Nano Lett.* **2012**, *12*, 3941−3947.
(27) Born, M.; Wolf, E. *Principles of Optics*; Cambridge University Press: Cambridge, U.K., 1999.
(28) Zhang, Q. F.; Chou, T. R.; Russo, B.; Jenekhe, S. A.; Cao, G. Z. Aggregation of ZnO Nanocrystallites for High Conversion Efficiency in Dye-Sensitized Solar Cells. *Angew. Chem., Int. Ed.* **2008**, *47*, 2402−2406.
(29) Wang, K. X.; Yu, Z.; Liu, V.; Cui, Y.; Fan, S. Absorption Enhancement in Ultrathin Crystalline Silicon Solar Cells with Antireflection and Light-Trapping Nanocone Gratings. *Nano Lett.* **2012**, *12*, 1616−1619.
(30) Fan, S.; Joannopoulos, J. D. Analysis of Guided Resonances in Photonic Crystal Slabs. *Phys. Rev. B* **2002**, *65*, 235112(1−8).
(31) Johnson, S. G.; Fan, S.; Villeneuve, P. R.; Joannopoulos, J. D.; Kolodziejski, L. A. Guided Modes in Photonic Crystal Slabs. *Phys. Rev. B* **1999**, *60*, 5751−5758.
(32) Munday, J. N.; Callahan, D. M.; Atwater, H. A. Light Trapping Beyond $4n^2$ Limit in Thin Waveguides. *Appl. Phys. Lett.* **2012**, *100*, 121121 (1−4).
(33) Green, M. A. Enhanced Evanescent Mode Light Trapping in Organic Solar Cells and Other Low Index Optoelectronic Devices. *Prog. Photovoltaics* **2011**, *19*, 473−477.
(34) Min, B.; Ostby, E.; Sorger, V.; Ulin-Avila, E.; Yang, L.; Zhang, X.; Vahala, K. High-Q Surface-Plasmon-Polariton Whispering-Gallery Microcavity. *Nature* **2009**, *457*, 455−458.
(35) Dabirian, A.; Akbari, M.; Mortensen, N. A. The Radiated Fields of the Fundamental Mode of Photonic Crystal Fibers. *Opt. Express* **2005**, *11*, 3999−4004.

DOI: 10.1021/acsami.5b03719
ACS Appl. Mater. Interfaces 2015, 7, 14926−14932